

# Size magnification as a complement to Cosmic Shear

B. Casaponsa,<sup>1,2\*</sup> A. F. Heavens<sup>3†</sup>, T. D. Kitching<sup>4‡</sup>, L. Miller<sup>5</sup>, R.B. Barreiro<sup>1</sup>,  
E. Martínez-González<sup>1</sup>

<sup>1</sup> *Instituto de Física de Cantabria, CSIC-Universidad de Cantabria, Avda. de los Castros s/n, 39005 Santander, Spain.*

<sup>2</sup> *Dpto. de Física Moderna, Universidad de Cantabria, Avda. de los Castros s/n, 39005 Santander, Spain.*

<sup>3</sup> *Imperial Centre for Inference and Cosmology, Imperial College, Blackett Laboratory, Prince Consort Road, London SW7 2AZ U.K.*

<sup>4</sup> *SUPA, Institute for Astronomy, University of Edinburgh, Blackford Hill, Edinburgh EH9 3HJ, U.K.*

<sup>5</sup> *Department of Physics, University of Oxford, Denys Wilkinson Building, Keble Road, Oxford OX1 3RH, U.K.*

Accepted ; Received ; in original form

## ABSTRACT

We investigate the extent to which cosmic size magnification may be used to complement cosmic shear in weak gravitational lensing surveys, with a view to obtaining high-precision estimates of cosmological parameters. Using simulated galaxy images, we find that size estimation can be an excellent complement, finding that unbiased estimation of the convergence field is possible with galaxies with angular sizes larger than the point-spread function (PSF) and signal-to-noise ratio in excess of 10. The statistical power is similar to, but not quite as good as, cosmic shear, and it is subject to different systematic effects. Application to ground-based data will be challenging, with relatively large empirical corrections required to account for biases for galaxies which are smaller than the PSF, but for space-based data with 0.1 arcsecond resolution, the size distribution of galaxies brighter than  $i \simeq 24$  is ideal for accurate estimation of cosmic size magnification.

**Key words:** data analysis - weak lensing- size magnification

## 1 INTRODUCTION

General Relativity predicts that the path of light is distorted when interacting with a gravitational field. This modification of the light paths is called gravitational lensing and is a powerful tool for probing the distribution of mass in the Universe. The variation of the light path depends on the position in the sky of the emitting object, the distance from the emitting object to the lens and the observer and on the potential along the light path. As the Universe is in permanent evolution photons that come from an earlier stage of the Universe will be deflected in a different way from those emitted in later stages (for a detailed reading see Schneider et al. 1992; Narayan & Bartelmann 1996; Mellier 1999; Munshi et al. 2008). Hence by studying the lensing observable distortion, a reconstruction of the three-dimensional unbiased distribution of matter (both light and dark) can be performed. The result is a picture of the Universe over time, therefore both the power spectrum and the growth of density perturbations with redshift can be inferred. Dark energy and modifications to Einstein gravity act to modify the lensing effect by changing the distance-

redshift relation and the growth of density perturbations (Huterer 2002; Munshi & Wang 2003). Therefore lensing effects are a source of valuable information for three of the important open issues in modern cosmology, namely the distribution of dark matter, the properties of dark energy and the nature of gravity.

The amount of gravitational lensing induced on the image of a background source is characterized by an image distortion matrix, which may be written in terms of the convergence  $\kappa$ , that is the field responsible for the changes in the image size and brightness, and the complex shear  $\gamma$  that, in the limit of small  $\kappa$ , parameterises the distortion of the shape. Observationally there are three main effects on the background sources: changes in the ellipticity, amplification in terms of flux, and magnification of the size. For large densities of (dark) matter the effects are all very strong, and multiple images of the background galaxies can be produced with large distortion. The studies of this distortion have led to local reconstruction of the distribution of non-baryonic matter for many years (Tyson et al. 1984). When the concentration of matter is not as high, the effects are not as obvious, and more difficult to detect. The lensed background source is observed with changes in the ellipticities, flux and size, but the effects are so small that, for a single galaxy, it is impossible to know if they are intrinsic

\* e-mail: casaponsa@ifca.unican.es

† e-mail: a.heavens@imperial.ac.uk

‡ e-mail: tdk@roe.ac.uk

properties of the galaxy or they are produced by lensing. However in this weak lensing limit on large scales, the distortions may be observed statistically using a large sample of sources.

In weak lensing, the most studied effect is the modification to the galaxy shape (complex ellipticity), a measure of the shear. The shape distortion has the main advantage that the intrinsic distribution of galaxy ellipticities is expected to be random, according to the cosmological principle. Therefore under this assumption the average complex ellipticity is zero. Weak lensing effects using galaxy ellipticities have been detected by several groups using different surveys and different methods, see for example Wittman et al. (2000); Semboloni et al. (2006); Jarvis et al. (2006); Benjamin et al. (2007); Schrabback et al. (2010). An important effort has been made to include and test many possible systematic effects on shape measurement (including the point spread function [PSF], instrumental noise, pixelization for example), and there are several algorithms that can measure shapes with varying degrees of accuracy such as KSB (Kaiser et al. 1995), KSB+ (Hoekstra et al. 1998) and its variants (Rhodes et al. 2000; Kaiser 2000) and shapelets (Bernstein & Jarvis 2002; Refregier & Bacon 2003; Kuijken 2006) amongst others. To test, in a blind way, the ability of methods to measure the shapes of galaxies a series of simulations have been created: STEP, GREAT08 and GREAT10, where several methods have been tested and compared systematically, an explanation of the methods and their performance are shown in Heymans et al. (2006); Massey et al. (2007); Bridle et al. (2010); Kitching et al. (2012) respectively. A novel Bayesian model fitting approach *lensfit* was presented in Miller et al. (2007), that includes PSF and pixelization effects, and was successfully applied by Kitching et al. (2010) to the STEP challenge images. Moving beyond measuring the shapes of galaxies, the amplification effect is usually quantified using the number of counts of a given flux (see for example Broadhurst et al. 1995; Hildebrandt et al. 2009, 2011); the number of observed galaxies at a given flux increases due to the weak lensing of the foreground galaxies, we do not study this further in this paper.

In contrast to galaxy ellipticity measurement, the size-magnification effect has not been studied in detail, possibly because the complicating effects of the PSF and pixelisation were thought to be too challenging. However, there are two reasons for revisiting size magnification as a potential tool for cosmology: one is that accurate shear estimation is itself very challenging, and size could add useful complementary information; the second is that methods devised for ellipticity estimation must deal with the PSF and pixelisation, and as a byproduct provide a size estimate, or a full posterior probability distribution for estimated size, which is currently ignored or marginalised over. In terms of signal-to-noise of shear or convergence estimation, the relative strengths of the methods depend on the prior distributions of ellipticity and size. The former has an r.m.s. of around 0.3-0.4; for bright galaxies, the Sloan Digital Sky Survey (SDSS) found that the size distribution of massive galaxies is approximately log-normal with  $\sigma \ln R \sim 0.3$ , and for less massive galaxies  $\sigma(\ln R) \sim 0.5$ , where  $R$  is the Petrosian half-light radius (Shen et al. 2003). For deeper space data the dispersion is modestly larger (Simard et al. 2002). Thus one might expect

a slightly a smaller S/N for lensing measurements based on size rather than ellipticity, but not markedly so. Furthermore, Bertin & Lombardi (2006) proposed a method based on the tight relation between sizes and the central velocity dispersion (the fundamental plane relation) to reduce the observable size variance. Huff & Graves (2011) applied a similar method to 55,000 galaxies of the SDSS catalogue, and find consistency with shear using the same sample. Also a detection with COSMOS HST survey using a revised version of the KSB method is claimed in Schmidt et al. (2012).

Revisiting the size magnification in detail is the aim of this paper. As we will show, to use size-magnification we require i) a large area survey to result in sufficiently high number densities of galaxies to overcome the intrinsic scatter, and ii) a consistently small PSF that does not destroy the size information of the observed galaxies. Both of these requirements can be met with a wide-area space-based survey, although some science may be possible from the ground. Space-based surveys such as Euclid<sup>1</sup> (Laureijs et al. 2011) should meet these requirements (large samples will be available, and the PSF size is smaller than typical galaxies), so the size information should be considered as a complementary cosmological probe to weak lensing ellipticity measurements.

One advantage of using the size information is that the magnification is directly related to the convergence field  $\kappa$ , which is in turn directly related to the weighted surface mass density, while  $\gamma$  is related to the differential surface mass density. Those different radial dependences can be very useful to lift any degeneracies (Rozo & Schmidt 2010), and combining the size magnification information with the shear will reduce the uncertainties on the reconstruction of the distribution of matter (Jain 2002; Rozo & Schmidt 2010; Vallinotto et al. 2011). All of the shear estimation methods referred to above already estimate the size of galaxies when calculating the ellipticities, so we expect to measure this additional information for free, given an accurate ellipticity measurement, but the accuracy of size information should not be taken for granted: it is important to know the uncertainties in size measurement, and how they propagate to a convergence field estimation. It is this question of how accurately one can measure the sizes of galaxies, that this paper will address.

The paper is organized as follows. First, in section 2 we will present the estimator that we will use, then a brief comment on the method and the characteristics of the simulated images. In section 3 the analysis and results are explained and finally we will summarize the conclusions in section 4.

## 2 METHOD

A good algorithm for ellipticity weak lensing analysis must be able to measure shapes or sizes with an accuracy of a few percent, taking into account any possible systematic errors as the distortion introduced by the PSF, shot noise or pixelization. Another requirement is that it should be fast because the statistical analysis will be made on large samples. This means that the algorithm development is chal-

<sup>1</sup> <http://www.euclid-ec.org>

lensing because of the dissonant requirements of both increased accuracy and increased speed as the required systematic level decreases. Several methods have been proposed and applied to weak lensing surveys, in particular several of these methods are described in the challenge reports of STEP, GREAT08 and GREAT10 (Heymans et al. 2006; Bridle et al. 2010; Kitching et al. 2012). These blind challenges have been critical in demonstrating that methods can achieve the required accuracy for upcoming surveys by creating simulations with controlled inputs against which results can be tested. Here we propose a very similar approach as the one presented in the GREAT10 challenge, we have used simulated galaxy images with different properties to measure the response of the size/convergence measurement under different conditions (corresponding to changes in the PSF, S/N and bulge fraction).

## 2.1 Estimator

If the intrinsic size of a galaxy  $s^s$  is magnified,  $s = \mu s^s$ , where to first order the magnification is related to the convergence like  $\mu = 1 + \kappa$ , then  $\kappa = \frac{s}{s^s} - 1$ . We can construct an estimator for  $\kappa$  in the weak field limit by assuming that the mean size value is not modified by lensing, i.e.,  $\langle s^s \rangle = \langle s \rangle$ :

$$\hat{\kappa} = \frac{s}{\langle s \rangle} - 1. \quad (1)$$

This assumption should be valid because  $\langle \kappa \rangle = 0$ . We cannot obtain accurate estimates of  $\kappa$  for a single galaxy, we can see that from the definition of the estimator, smaller galaxies than the mean will always give a negative  $\hat{\kappa}$ , while larger galaxies will produce positive  $\hat{\kappa}$ . What is important is to test if our estimator is unbiased over a population to a sufficient degree to be useful for real data.

## 2.2 lensfit

Throughout we use *lensfit* (Miller et al. 2007; Kitching et al. 2008; Miller et al. 2012) to estimate the galaxy size; we use this because: 1) it has been shown that *lensfit* performs well on ellipticity measurement; 2) it is a model fitting code such that it measures the sizes of galaxies (that are part of the model); 3) it allows for the consistent investigation of the intrinsic distribution of galaxy sizes through the inclusion of a prior on size, and 4) it includes the effects of PSF and pixellisation. *lensfit* was proposed in Miller et al. (2007) and has been proved to be a successful tool for galaxy ellipticity shape measurements (Kitching et al. 2008). Although model-fitting is the optimal approach for this type of problem if the model used is an accurate representation of the data, the main disadvantage is that is usually computationally demanding to explore a large parameter space. *lensfit* solves this problem by analytically marginalizing over some parameters that are not of interest for weak lensing ellipticity measurements, such as position, surface brightness and bulge-fraction. The size reported by *lensfit* is also marginalised over the galaxy ellipticity.

### 2.2.1 Sensitivity correction

Miller et al. (2007) introduced the shear sensitivity, a factor that corrects for the fact that the code measures ellipticity

ties but that shear (a statistical change in ellipticity) is the quantity of interest. A similar correction is required for size measurement, whereby we measure the size but it is the convergence that is the quantity of interest; this correction is needed because for a single galaxy the prior information for the convergence is not known, and we assume it is zero. With a Bayesian method we can estimate the magnitude of this effect for each galaxy, a further reason to use a Bayesian model fitting code in these investigations. Consider the Bayesian estimate of the size of galaxy  $i$  and write its dependence on  $\kappa$  as a Taylor expansion:

$$\hat{s}_i = s_i^s + \kappa \frac{d\hat{s}_i}{d\kappa}, \quad (2)$$

In the simplistic case where the likelihood  $\mathcal{L}(s)$  is described by a Gaussian distribution with variance  $b^2$ , with an expected value  $s$ , and a prior  $\mathcal{P}(s)$  that also follows a Gaussian distribution centred on  $\bar{s}$  with variance  $a^2$ , then the posterior probability will follow a Gaussian distribution with expected value:

$$\langle s \rangle = \frac{\bar{s}b^2 + s_d a^2}{a^2 + b^2}$$

and variance

$$\sigma^2 = \frac{a^2 b^2}{a^2 + b^2}$$

Note that here  $s$  stands for the fitted model parameter for the size explained in Sec. 2.3, and  $s_d$  is the data. These equations illustrate that the posterior is driven towards the prior in the low S/N limit ( $b \rightarrow \infty$ ), and thus requires correction. Differentiating the expression  $s_d = s^s(1 + \kappa)$  we find that the  $\kappa$  sensitivity correction is:

$$\frac{d\hat{s}}{d\kappa} = \frac{a^2}{a^2 + b^2} \frac{ds_d}{d\kappa} = \frac{a^2}{a^2 + b^2} s^s, \quad (3)$$

substituting into eq. 2

$$\hat{s}_i = s_i^s + \kappa s_i^s \frac{a^2}{a^2 + b^2}$$

we find the estimator for  $\kappa$  will be the same as in eq. 1, corrected by the sensitivity factor:

$$\kappa = \left( \frac{\hat{s}}{\langle \hat{s} \rangle} - 1 \right) \frac{a^2 + b^2}{a^2}. \quad (4)$$

In this work we have used this approximation for simplicity but in general a normal distribution should not be assumed. A more general estimation of the  $\kappa$  correction can be done in the same way as with the shear and can be evaluated numerically, without the need of using external simulations.

To calculate the sensitivity correction in the general case we consider the response of the posterior to a small  $\kappa$ ,  $\mathcal{L}(s - s^s) \mapsto \mathcal{L}(s - s^s - \kappa s^s)$  and expand it as a Taylor series:

$$\mathcal{L}(s - s^s - \kappa s^s) \simeq \mathcal{L}(s - s^s) - s^s \kappa \frac{d\mathcal{L}}{ds}.$$

We then substitute into

$$\langle s \rangle = \frac{\int s \mathcal{P}(s) \mathcal{L}(s) ds}{\int \mathcal{P}(s) \mathcal{L}(s) ds}$$

and differentiate to obtain the analytic expression for the

$\kappa$  sensitivity (for more details of this applied to ellipticity measurement see Miller et al. 2007; Kitching et al. 2008)

$$\frac{ds}{d\kappa} \simeq \frac{\int (\langle s \rangle - s) \mathcal{P}(s) s^s \frac{d\mathcal{L}}{ds} ds}{\int \mathcal{P}(s) \mathcal{L}(s) ds}. \quad (5)$$

If the prior and likelihood are described by a normal distribution, this expression can be analytically computed and the sensitivity correction is the same as before. A similar empirically motivated correction on the estimator expression is used in Eq.5 of Schmidt et al. (2012), where the factor is computed with simulations.

### 2.3 Simulations

In order to test the estimation of sizes with *lensfit* we have generated the same type of simulations used in the GREAT10 challenge (Bridle et al. 2010; Kitching et al. 2010, 2012), but with non-zero  $\kappa$ . Multiple images were generated, each containing 10,000 simulated galaxies in a grid of 100x100 postage stamps of 48x48 pixels; each postage stamp contains one galaxy.

Each galaxy is composed of a bulge and a disk, each modelled with Sérsic light profiles:

$$I(r) \simeq I_0 \exp \left\{ -K \left[ \left( \frac{r}{r_d} \right)^{\frac{1}{n}} - 1 \right] \right\} \quad (6)$$

where  $I_0$  is the intensity at the effective radius  $r_d$  that encloses half of the total light and  $K = 2n - 0.331$ . The disks were modelled as galaxies with an exponential light profile ( $n = 1$ ), and the bulges with a de Vaucouleurs profile ( $n = 4$ ). Ellipticities for bulge and disk were drawn from a Gaussian distribution centred on zero with dispersion  $\sigma = 0.3$ . Both components were centred in the postage stamp with a Gaussian distribution of  $\sigma = 0.5$  pixels. The galaxy image was then created adding both components. The S/N was fixed for all galaxies of the image and the implementation is the same as in Kitching et al. (2012). Finally the PSF was modeled with a Moffat profile with  $\beta = 3$ , with FWHM fixed for all galaxies on the image, with different ellipticities, drawn from a uniform distribution, with ranges given in Table. 1.

We have generated 4 different sets of images, whose detailed information is given in Table. 1. The different types of image were generated to study the effects of the bulge fraction (fraction of the total flux concentrated in the bulge), the S/N and the PSF separately. In summary, the main characteristics of the considered sets are:

- Set 1. Disk-only galaxies, (bulge fraction = 0), negligible PSF effect (FWHM PSF = 0.01 pixels) and different S/N.
- Set 2. Disk-only galaxies, (bulge fraction = 0), with S/N=20 and different sizes of PSF.
- Set 3. Negligible PSF effect, S/N=20 and different bulge fractions.
- Set 4. Bulge fraction of 0.5, FWHM of PSF 1.5 times smaller than the characteristic size of the disk, and different S/N.

To characterize the size of the galaxy the half-light disk radius,  $s = r_d$  is used. We have drawn a Gaussian distribution for  $r_d$ , with expected value of 7 pixels and dispersion of 1.2 pixels, to keep disk sizes of at least 2 pixels and not larger

that the postage-stamp. The galaxy sizes explored here have a somewhat smaller range ( $\sigma(\ln R) \sim 0.18$ ) than found by Shen et al. (2003) with the SSDS catalogue, where in terms of pixels the mean value of the full sample is around 5 with  $\sigma(\ln R) \sim 0.3$  (see Fig.1 of Shen et al. (2003)). Therefore the sensitivity corrections are consequently larger than would be needed for real data. Besides a wider distribution of galaxies, the important change from the original images for the GREAT10 challenge is the addition of a non-zero kappa-field that creates a size-magnification effect (in GREAT10 only a shear field was used to distort the intrinsic galaxy images). A Gaussian convergence field with a simple power-law power spectrum of  $P_k \propto 10^{-5} l^{-1.1}$  has been applied to each image using the flat-sky approximation. The power-law is good approximation to the theoretical power spectrum over the scales  $10 \leq l \leq 1000$  (see i.e. Huterer 2002).

## 3 RESULTS

Before trying to estimate the convergence field of our most realistic image, we have tested the dependence on different aspects separately: S/N, PSF size and bulge-fraction. We expect these to be the observable effects that have the largest impact on the ability to measure the size of galaxies. Lower S/N will cause size estimates to become more noisy and possibly biased (in a similar way as for ellipticity, see Melchior & Viola 2012); a larger PSF size will act to remove information on galaxy size from the image and a change in galaxy type or bulge-fraction may cause biases because now two characteristic sizes are present in the images (bulge and disk lengths). In order to study carefully the sensitivity of our estimator to systematic noise, PSF or galaxy properties, we started from the simplest case and added increasing levels of complexity. The number of galaxies used for the analysis is 200,000 for the first three sets and we increased the number to 500,000 for the last test to give smaller error bars.

We compare the estimated  $\hat{\kappa}$  computed as in Eq. 1 with the input field  $\kappa$ , and fit a straight line to the relationship to estimate a multiplicative bias  $m$  and an additive bias  $c$ :

$$\hat{\kappa} = (m + 1)\kappa + c. \quad (7)$$

To obtain  $m$  and  $c$  values, we estimate the observed size of each galaxy, and compute  $\hat{\kappa}$  using the estimator in Eq. 1. The sensitivity correction is applied as explained in Sec. 2.2.1. Then we compare the corrected estimated  $\kappa$  of each galaxy with the original convergence field introduced. Finally we bin the data<sup>2</sup> and a linear fit is done to compute  $m$  and  $c$ . This process is shown in Fig. 1.

We now discuss each of the categories in turn.

### 3.1 Signal-to-noise

As a first approach to the problem, disk-only galaxies with a negligible PSF (FWHM = 0.01 pixels) and zero ellipticity were generated to test the sensitivity on the S/N only given

<sup>2</sup> Note that the differences between the results before and after the binning of  $\kappa$  are within the errorbars.

Set Name	S/N	<i>fwhm</i> PSF	<i>e</i> PSF	B/D fraction	$r_d$	$r_b$	<i>e</i>
Set 1	<b>[10,40]</b>	0.01	0	0	$\langle r_d \rangle = 7, \sigma = 1.2$	-	0
Set 2	20	<b>[0.01,10]</b>	0	0	$\langle r_d \rangle = 7, \sigma = 1.2$	-	$\langle e \rangle = 0, \sigma = 0.3$
Set 3	20	0.01	0	<b>[0,0.95]</b>	$\langle r_d \rangle = 7, \sigma = 1.2$	$r_d/2$	$\langle e \rangle = 0, \sigma = 0.3$
Set 4	<b>[10,40]</b>	4.5	<b>[-0.1,0.1]</b>	0.5	$\langle r_d \rangle = 7, \sigma = 1.2$	$\langle r_b \rangle = 3.5, \sigma = 0.6$	$\langle e \rangle = 0, \sigma = 0.3$

**Table 1.** Major characteristics of the different sets used in this analysis. In bold are marked the variables explored in each set and the range of variation. In Set 4, PSF ellipticities are drawn from a uniform distribution in the range specified. Note that  $r_i$  corresponds to the half-light radius. Last column is the galaxy ellipticity and is the same for both components, bulge and disk.

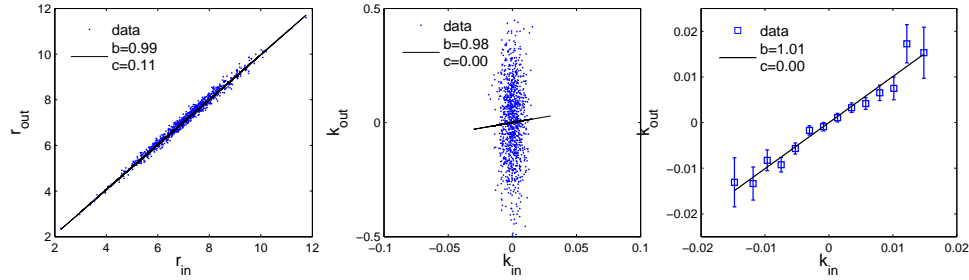


**Figure 1.** Sequence of steps to obtain  $m$  and  $c$  values. First panel shows the *lensfit* output size compared to the input size, in the second panel the estimated  $\kappa$  compared to the input convergence at each galaxy, and in the third panel is shown the same plot using bins. Slope and intercept values of the fitting are shown in each plot (Throughout, we fit generically  $y = bx + c$ , with  $b = m + 1$  and  $c = c$  of eq. 7). This is for galaxies of Set 1 with signal-to-noise 40.

otherwise perfect data. In Fig. 2 we can see that as we increase the S/N the accuracy of the size estimation grows, as expected. In Fig. 3 we show the estimation of the convergence field, corrected by the sensitivity correction. Although the range of the output and input values differs by almost one order of magnitude, there is a clear correlation between the inputs and the outputs, and the slope is close to unity for all S/N explored. In Fig. 4 the estimates for  $m$  and  $c$  are shown, with the sensitivity correction and without it. In this case the correction does not alter much the results except for low S/N, because the sizes are less accurately estimated. In this paper the factor  $a^2/(a^2 + b^2)$  is estimated by the inverse of the slope of the size estimation fitting (see Fig. 2). Using 200,000 galaxies for this test, the values found for  $m$  and  $c$  are consistent with zero, typically  $m \simeq 0.02 \pm 0.05$ , and  $c \simeq (5 \pm 5) \times 10^{-4}$ .

### 3.2 PSF effect

To study the uncertainties on the size estimation due to the PSF size, we generated images with different FWHM PSF values, with an intermediate signal to noise (S/N=20), maintaining the same properties as before, except that we considered here a Gaussian distribution of ellipticities with mean value of  $e = 0$  and  $\sigma_e = 0.3$  (per component). The size estimates are good for small PSFs, but become progressively more biased as the PSF size increases beyond the disk scale length (see Fig. 5). A PSF with a FWHM larger or similar to the size of the disk, tends to make the galaxy look larger, and the estimator for  $\kappa$  is biased. This effect can be seen in the slope and intercept of  $\hat{\kappa}$  vs  $\kappa$  plot (Fig. 6). Fig. 7 shows the variation of the parameters  $m$  and  $c$  with the ratio between the scale-length of the PSF and the galaxy (ratio= $r_d/PSF_{FWHM}$ ).

We find no evidence for an additive bias, but we do find a multiplicative bias for large PSFs. With a wide size dis-

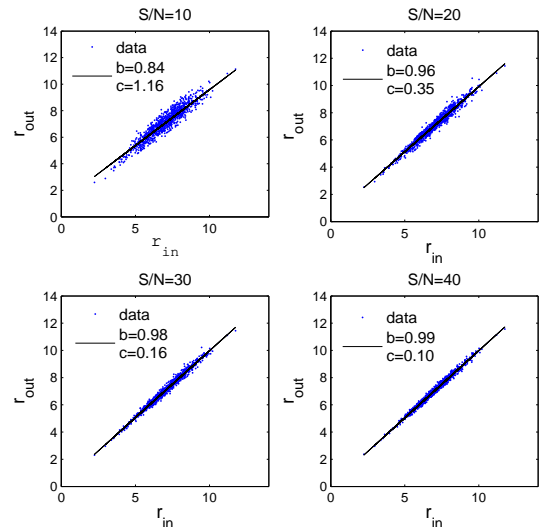


**Figure 2.** Comparison of the estimated sizes by *lensfit* with the input galaxy size for different S/N in the range [10,40]. Disk-only circular galaxies with a negligible PSF effect are considered (Set 1). Slope and intercept of the fitting are shown ( $b$  and  $c$ , respectively). Note that the input size is the lensed one.

tribution, some of the smaller galaxies are convolved with a PSF larger than its size, and this could produce an overall bias in  $\kappa$ , but if the number is not very large, this will not affect the global estimation of the convergence field. Similar biases exist with shear for large PSFs, but the biases are larger here. For a space-based experiment, with a relatively bright cut at  $i \sim 24$ , such as planned for Euclid, the limitation on PSF size will not be a problem, as the median galaxy size is 0.24 arcsec (Simard et al. 2002; Miller et al. 2012), comfortably larger than the PSF FWHM of 0.1 arcsec. For

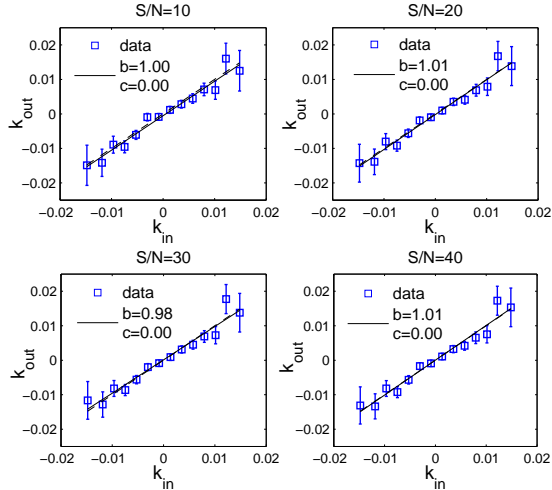


**Figure 3.** Comparison of the binned estimated convergence and the input value for Set 1 with different S/N in the range [10,40]. Slope and intercept of the fitting are shown ( $b$  and  $c$ , respectively). For errors, see text.

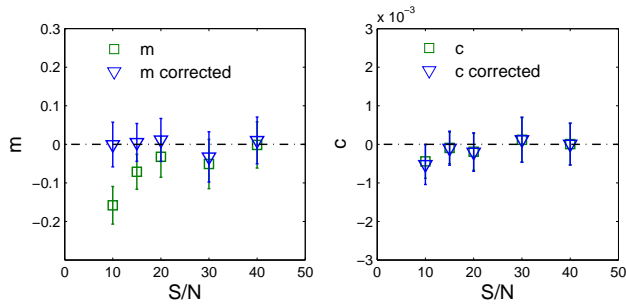


**Figure 4.**  $m$  and  $c$  values computed with 200,000 galaxies of Set 1. Triangles are for the values obtained with the sensitivity correction and squares without it.

ground-based surveys, such as CFHTLenS and future experiments the situation is not so clear, the measurement will be more challenging, and large empirical bias corrections of the order of  $m \simeq -0.5$  will be needed (see the first point of Fig. 7).

### 3.3 Bulge fraction

In this test we generated galaxy images with bulges with different fractions of the total flux, to test the response to the galaxy type. In Fig. 8 we show that galaxy size estimates for a bulge fraction of 0.2 is much better than for galaxies with bulge-fraction of 0.95. This is because for bulge dominated models the central part of the galaxy becomes under sampled due to a limiting pixel scale. The poor estimation of sizes is reflected in the  $\kappa$  estimation (Fig. 9).

The parameters  $m$  and  $c$  for this set are shown in Fig. 10, where we can see that for bulge-fraction greater than 0.8, the results are clearly biased ( $m = -0.25$ ). For all bulge-fractions the error bars are around 10%.

Although for bulge-only galaxies, the  $\kappa$  estimates are poor, most of the galaxies used for weak lensing exper-

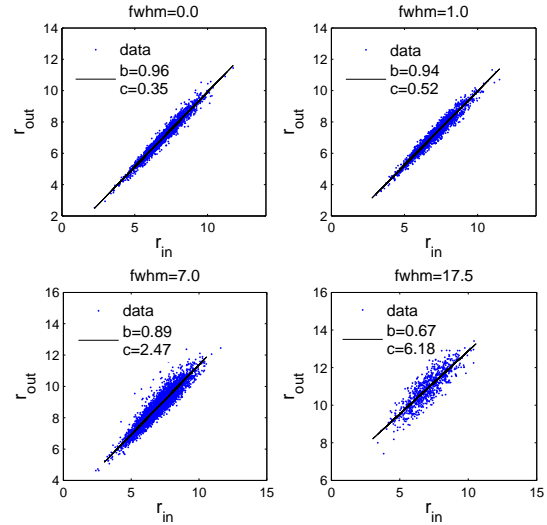


**Figure 5.** Sizes estimates vs input sizes for four different PSF scale-lengths between 0.1 and 7 pixels. Galaxies are disks with S/N=20 and mean size 7 pixels. Slope and intercept of the fitting are shown ( $b$  and  $c$ , respectively).

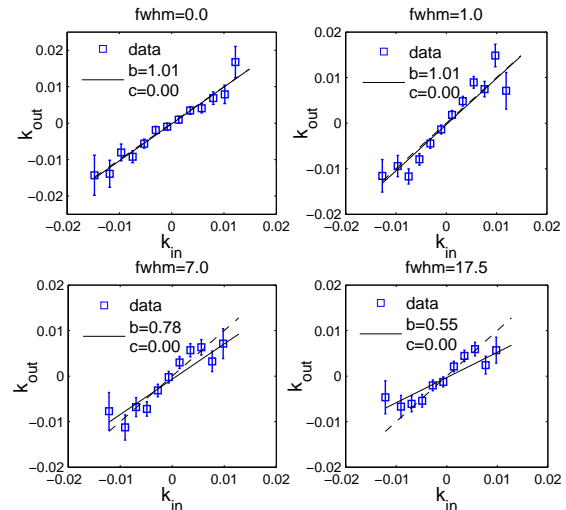


**Figure 6.**  $\kappa$  estimates vs input values for four different PSF scale-lengths. Galaxies are disks with S/N=20 and mean size 7 pixels. Dashed line is  $\kappa_{out} = \kappa_{in}$  and the solid line is the least squares fit, with slope and intercept shown in the plots. Note that  $b=m+1$ .

iments have bulge fractions lower than 0.5 (Schade et al. 1996), then the useful population can be large enough to do a successful analysis.

### 3.4 Most Realistic Set

The last set includes realistic values for all the effects we investigate. We have generated elliptical galaxies with a bulge fraction of 0.5 convolved with an anisotropic PSF with FWHM of 4.5 pixels (1.5 times smaller than the characteristic scale-length of the disk), and again we investigate the dependence on S/N. This is also a challenging test for *lensfit*,

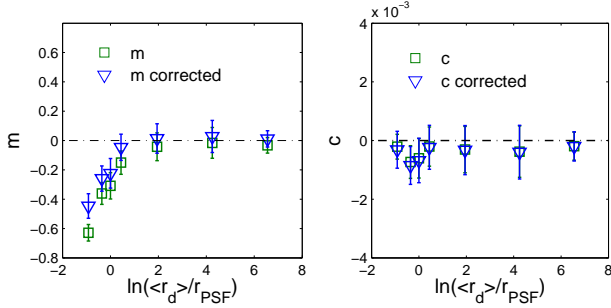


**Figure 7.**  $m$  and  $c$  values computed with 200,000 galaxies of Set 2. Triangles represent the values obtained with the sensitivity correction and squares without it.

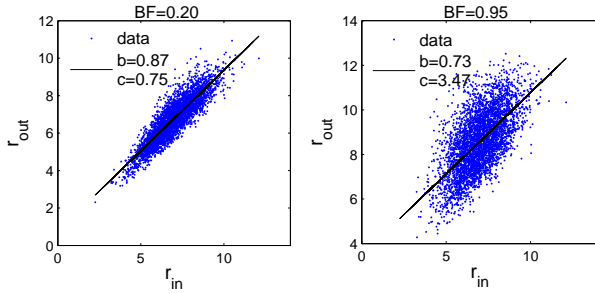


**Figure 8.** Sizes estimates vs input sizes for different bulge fractions in the range  $[0.2, 0.95]$ . Bulge+Disk elliptical galaxies are used, with  $S/N=20$  and negligible effect of the PSF (Set3). Slope and intercept of the fitting are shown ( $b$  and  $c$ , respectively).

the current version of which uses a simplified parameter set where the bulge scale length is assumed to be half the disk scale length. Here, we include a dispersion in the bulge scale length of 0.6 pixels around a mean value of 3.5 pixels. The analysis was done with 500,000 galaxies, to keep the error bars smaller than 10%. In Fig. 11 are shown the values of  $m$  and  $c$  for this set, with and without the sensitivity correction. If we compare it with the previous plots we can see that as the galaxies get more realistic the importance of the correction increases. Results for this set are shown in Fig. 11, showing unbiased results except for  $S/N=10$ , which has  $m = -0.19 \pm 0.1$ . For the higher  $S/N$  points, we find  $|m| < 0.06$  with errorbars of  $\pm 0.09$ .

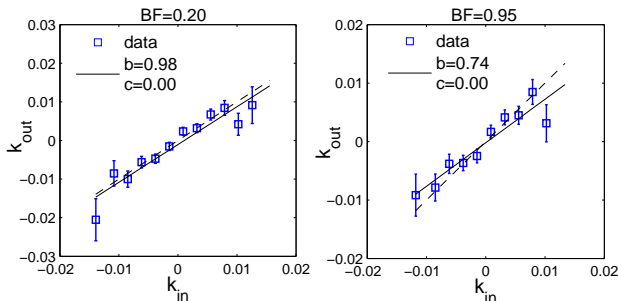


**Figure 9.**  $\kappa$  estimates vs input values for two different bulge fractions  $[0.2, 0.95]$ . Bulge+Disk elliptical galaxies with  $S/N$  of 20 and negligible effect of the PSF (Set 3). Dashed line is  $\kappa_{out} = \kappa_{in}$  and the solid line is the fit of the output values. Note that  $b=m+1$  of eq. 7.

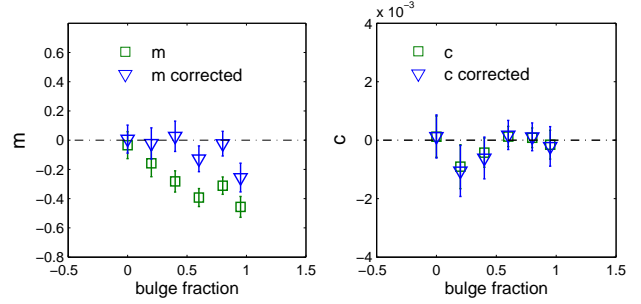


**Figure 10.**  $m$  and  $c$  values computed with 200,000 galaxies of Set 3. Values obtained with the sensitivity correction are marked by triangles and by squares are without the correction.

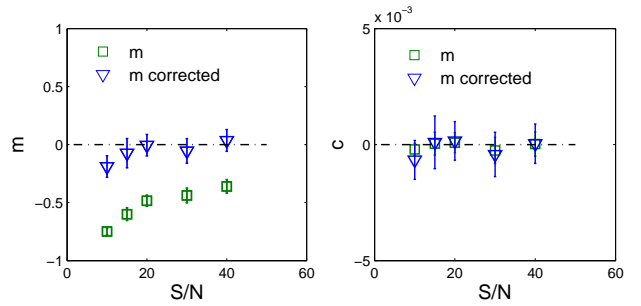


**Figure 11.**  $m$  and  $c$  parameters for 500,000 galaxies of Set 4. Squares are raw  $m$  and  $c$  values; triangles have the sensitivity correction included.

#### 4 CONCLUSIONS AND DISCUSSIONS

In this paper we present the first systematic investigation of the performance of a weak lensing shape measurement methods' ability to estimate the magnification effect through an estimate of observed galaxy sizes. We performed this test by creating a suite of simulations, with known input values, and by using the most advanced shape measurement available at the current time, *lensfit*.

A full study of the magnification effect using sizes was performed testing the dependence on  $S/N$ , PSF size and type of galaxy. The requirements on biases on shear (or equivalently convergence) for Euclid, so that systematics do not dominate the very small statistical errors in cosmological parameters are stringent: the multiplicative and additive biases are required to be  $|m| \leq 2 \times 10^{-3}$  and  $|c| \leq 10^{-4}$ . A much larger study will be required to determine whether these requirements can be met for size, but we find in this study no evidence for additive biases at all, and no evidence for multiplicative bias provided that the PSF is small enough ( $< \text{galaxy scalelength}/1.5$ ), the  $S/N$  high enough ( $\geq 15$ ), and the bulge not too dominant (bulge/disk ratio  $< 4$ ). We find that if the disk is faint in comparison to the bulge (bulge/disk ratio  $\geq 1.5$ ), the estimation of the half-light disk radius is biased. This effect increases with the bulge/disk ratio, and we find that the bias in the convergence estimation can be important for bulge fraction  $> 0.8$ .

Besides instrumental and environmental issues, there can be astrophysical contaminants associated with weak lensing. In the case of shape distortion, the first assumption that galaxy pairs have no ellipticity correlation is



not entirely accurate. There are intrinsic alignments of nearby galaxies due to the alignment of angular momentum produced by tidal shear correlations (II correlations, see for detections Brown et al. (2002); Heymans et al. (2004); Mandelbaum et al. (2011); Joachimi et al. (2011, 2012), and for theory Heavens et al. (2000); Catelan & Porciani (2001); Crittenden et al. (2001); Heymans & Heavens (2003)). In addition there can be correlations between density fields and ellipticities (GI correlations, Hirata & Seljak (2004); Mandelbaum et al. (2006)). These intrinsic correlations have been studied in detail and it is not trivial to account for or remove them when quantifying the weak lensing signal.

The intrinsic correlation of sizes and its dependence on the environment, are still open issues. In fact, the correlation of sizes and density field, is known to play an important role in discriminating between models of size evolution; recent work finds a significant correlation between sizes and the density field using around 11,000 galaxies drawn from the joint DEEP2/DEEP3 data-set (Cooper et al. 2012; Papovich et al. 2012), while earlier studies with smaller samples have been in disagreement. Using 5,000 galaxies of STAGES data-set, Maltby et al. (2010) find a possible anti-correlation between density field and size for intermediate/low-mass spiral galaxies. Clustered galaxies seem to be 15% smaller than the ones in the field, while they do not find any correlation for high-mass galaxies. Also for massive elliptical galaxies from ESO Distant Clusters Survey, Rettura et al. (2010) do not find any significant correlation, while using the same data set Cimatti et al. (2012) claims a similar correlation as in Cooper et al. (2012). In Park & Choi (2009) they study the correlation between sizes and separation with late and early-type galaxies from SSDS catalogue, at small and large scales. They compare the size of the nearest neighbour with the separation between them, and find larger galaxies at smaller separations. This correlation is found for early-type galaxies if the separation between the galaxies is smaller than the merging scale, but not for larger separations. The size of late-type galaxies seems not to have a correlation with the separation in any scale. We expect that further studies with larger samples will clarify the intrinsic correlations of sizes, we note that the systematics are generated from different physical processes than in the case of shear and so will affect the signal in a different way; we suggest this is a positive, and another reason why a joint analysis of ellipticity and sizes is interesting.

The analysis presented here has assumed that the statistical distribution of galaxy sizes is known, whereas in practice the size distribution depends on galaxy brightness and must be determined from observation. Gravitational lensing of a galaxy with amplification  $A$  increases both the integrated flux and area of that galaxy by  $A$ , which has the effect of moving galaxies along a locus of slope 0.5 in the relation between  $\log(\text{size})$  and  $\log(\text{flux})$ . Thus, if the intrinsic distribution of sizes  $r$  of galaxies scales with flux  $S$  as  $r \propto S^\beta$ , the apparent shift in size caused by lensing amplification  $A$  is  $r' \propto A^{0.5-\beta}$ , resulting in a dilution of the signal compared with the idealised case investigated in this paper. A similar effect occurs in galaxy number magnification, where the observed enhancement in galaxy number density  $N'$  varies as  $N' \propto A^{\alpha-1}$ , if the intrinsic number density of galaxies varies as  $N \propto S^{-\alpha}$  (Broadhurst et al. 1995). The value of  $\beta$  at faint magnitudes has recently been estimated

by Miller et al. (2012), who analysed the fits to galaxies with  $i \lesssim 25$  of Simard et al. (2002) and estimated  $\beta \simeq 0.29$ . Thus we expect this effect in a real survey to dilute the lensing magnification signal by a factor 0.42, but still allowing detection of lensing magnification. In practice, the dilution factor could be evaluated by fitting to the size-flux relation in the lensing survey.

Lensing number magnification surveys are also affected by the problem that varying Galactic or extragalactic extinction reduces the flux of galaxies and thus may cause a spurious signal (e.g. Ménard et al. 2010). Such extinction would also affect the size magnification of galaxies, but with a different sign in its effect. Thus a combination of lensing number magnification and size magnification might be very effective at removing the effects of extinction from magnification analyses.

Space-based surveys as Euclid should overcome the limitations that we have exposed here, having a large number of galaxies, with  $S/N > 10$ , and importantly a PSF at least 1.5 smaller than the average disk size. The addition of the size information to the ellipticity analysis is expected to reduce the uncertainties in the estimation of weak lensing signal, and therefore improve the constraints of the distribution of matter and dark energy properties.

## ACKNOWLEDGMENTS

We thank Catherine Heymans for interesting discussions. BC thanks the Spanish Ministerio de Ciencia e Innovación for a pre-doctoral fellowship. We acknowledge partial financial support from the Spanish Ministerio de Economía y Competitividad AYA2010-21766-C03-01 and Consolider-Ingenio 2010 CSD2010-00064 projects. TDK is supported by a Royal Society University Research Fellowship. The authors acknowledge the computer resources at the Royal Observatory Edinburgh. The author thankfully acknowledges the computer resources, technical expertise and assistance provided by the Advanced Computing & e-Science team at IFCA.

## REFERENCES

- Benjamin J., Heymans C., Semboloni E., van Waerbeke L., Hoekstra H., Erben T., Gladders M. D., Hettterscheidt M., Mellier Y., Yee H. K. C., 2007, *MNRAS*, 381, 702
- Bernstein G. M., Jarvis M., 2002, *AJ*, 123, 583
- Bertin G., Lombardi M., 2006, *ApJL*, 648, L17
- Bridle S., Balan S. T., Bethge M., Gentile M., Harmeling S., Heymans C., Hirsch M., Hosseini R., Jarvis e. a., 2010, *MNRAS*, 405, 2044
- Broadhurst T. J., Taylor A. N., Peacock J. A., 1995, *ApJ*, 438, 49
- Brown M. L., Taylor A. N., Hambly N. C., Dye S., 2002, *MNRAS*, 333, 501
- Catelan P., Porciani C., 2001, *MNRAS*, 323, 713
- Cimatti A., Nipoti C., Cassata P., 2012, *MNRAS*, 422, L62
- Cooper M. C., Griffith R. L., Newman J. A., Coil A. L., Davis M., Dutton A. A., Faber S. M., Guhathakurta P., Koo D. C., Lotz J. M., Weiner B. J., Willmer C. N. A., Yan R., 2012, *MNRAS*, 419, 3018



- Crittenden R. G., Natarajan P., Pen U.-L., Theuns T., 2001, *ApJ*, 559, 552
- Heavens A., Refregier A., Heymans C., 2000, *MNRAS*, 319, 649
- Heymans C., Brown M., Heavens A., Meisenheimer K., Taylor A., Wolf C., 2004, *MNRAS*, 347, 895
- Heymans C., Heavens A., 2003, *MNRAS*, 339, 711
- Heymans C., Van Waerbeke L., Bacon D., Berge J., Bernstein G., Bertin E., Bridle S., Brown M. L., et al. 2006, *MNRAS*, 368, 1323
- Hildebrandt H., Muzzin A., Erben T., Hoekstra H., Kuijken K., Surace J., van Waerbeke L., Wilson G., Yee H. K. C., 2011, *ApJL*, 733, L30
- Hildebrandt H., van Waerbeke L., Erben T., 2009, *A&A*, 507, 683
- Hirata C. M., Seljak U., 2004, *Phys.Rev.D*, 70, 063526
- Hoekstra H., Franx M., Kuijken K., Squires G., 1998, *ApJ*, 504, 636
- Huff E. M., Graves G. J., 2011, *arXiv:astro-ph/1111.1070*
- Huterer D., 2002, *Phys.Rev.D*, 65, 063001
- Jain B., 2002, *ApJL*, 580, L3
- Jarvis M., Jain B., Bernstein G., Dolney D., 2006, *ApJ*, 644, 71
- Joachimi B., Mandelbaum R., Abdalla F. B., Bridle S. L., 2011, *A&A*, 527, A26
- Joachimi B., Semboloni E., Bett P. E., Hartlap J., Hilbert S., Hoekstra H., Schneider P., Schrabback T., 2012, *ArXiv e-prints*
- Kaiser N., 2000, *ApJ*, 537, 555
- Kaiser N., Squires G., Broadhurst T., 1995, *ApJ*, 449, 460
- Kitching T., Balan S., Bernstein G., Bethge M., Bridle S., Courbin F., Gentile M., Heavens A., Hirsch M., Hosseini R., Kiessling A., Amara A., Kirk D., Kuijken e. a., 2010, *arXiv:astro-ph/1009.0779*
- Kitching T. D., Balan S. T., Bridle S., Cantale N., Courbin F., Eifler T., Gentile M., Gill M. S. S., Harmeling S., Heymans e. a., 2012, *MNRAS*, 423, 3163
- Kitching T. D., Miller L., Heymans C. E., van Waerbeke L., Heavens A. F., 2008, *MNRAS*, 390, 149
- Kuijken K., 2006, *A&A*, 456, 827
- Laureijs R., Amiaux J., Arduini S., Auguères J. ., Brinchmann J., Cole R., Cropper M., Dabin C., Duvet L., Ealet A., et al. 2011, *arXiv:astro-ph/1110.3193L*
- Maltby D. T., Aragón-Salamanca A., Gray M. E., Barden M., Häußler B., Wolf C., Peng C. Y., Jahnke K., McIntosh D. H., Böhm A., van Kampen E., 2010, *MNRAS*, 402, 282
- Mandelbaum R., Blake C., Bridle S., Abdalla F. B., Brough S., Colless M., Couch e. a., 2011, *MNRAS*, 410, 844
- Mandelbaum R., Hirata C. M., Ishak M., Seljak U., Brinkmann J., 2006, *MNRAS*, 367, 611
- Massey R., Heymans C., Bergé J., Bernstein G., Bridle S., Clowe D., Dahle H., Ellis R., Erben T., Hetterscheidt M., High F. W., Hirata C. e. a., 2007, *MNRAS*, 376, 13
- Melchior P., Viola M., 2012, *MNRAS*, 424, 2757
- Mellier Y., 1999, *ARA&A*, 37, 127
- Ménard B., Scranton R., Fukugita M., Richards G., 2010, *MNRAS*, 405, 1025
- Miller L., e. a., 2012, submitted to *MNRAS*
- Miller L., Kitching T. D., Heymans C., Heavens A. F., van Waerbeke L., 2007, *MNRAS*, 382, 315
- Munshi D., Valageas P., van Waerbeke L., Heavens A., 2008, *Phys.Rep.*, 462, 67
- Munshi D., Wang Y., 2003, *ApJ*, 583, 566
- Narayan R., Bartelmann M., 1996, *arXiv:astro-ph/9606001*
- Papovich C., Bassett R., Lotz J. M., van der Wel A., Tran K.-V., Finkelstein S. L., Bell E. F., Conselice C. J., Dekel A., Dunlop J. S., Guo Y., et al. 2012, *ApJ*, 750, 93
- Park C., Choi Y.-Y., 2009, *ApJ*, 691, 1828
- Refregier A., Bacon D., 2003, *MNRAS*, 338, 48
- Rettura A., Rosati P., Nonino M., Fosbury R. A. E., Gobat R., Menci N., Strazzullo V., Mei S., Demarco R., Ford H. C., 2010, *ApJ*, 709, 512
- Rhodes J., Refregier A., Groth E. J., 2000, *ApJ*, 536, 79
- Rozo E., Schmidt F., 2010, *arXiv:astro-ph/1009.5735*
- Schade D., Lilly S. J., Le Fevre O., Hammer F., Crampton D., 1996, *ApJ*, 464, 79
- Schmidt F., Leauthaud A., Massey R., Rhodes J., George M. R., Koekemoer A. M., Finoguenov A., Tanaka M., 2012, *ApJL*, 744, L22
- Schneider P., Ehlers J., Falco E. E., 1992, *Gravitational Lenses*
- Schrabback T., Hartlap J., Joachimi B., Kilbinger M., Simon P., Benabed K., Bradač M., Eifler T. e. a. ., 2010, *A&A*, 516, A63
- Semboloni E., Mellier Y., van Waerbeke L., Hoekstra H., Tereno I., Benabed K., Gwyn S. D. J., Fu L., Hudson M. J., Maoli R., Parker L. C., 2006, *A&A*, 452, 51
- Shen S., Mo H. J., White S. D. M., Blanton M. R., Kauffmann G., Voges W., Brinkmann J., Csabai I., 2003, *MNRAS*, 343, 978
- Simard L., Willmer C. N. A., Vogt N. P., Sarajedini V. L., Phillips A. C., Weiner B. J., Koo D. C., Im M., Illingworth G. D., Faber S. M., 2002, *ApJS*, 142, 1
- Tyson J. A., Valdes F., Jarvis J. F., Mills Jr. A. P., 1984, *ApJL*, 281, L59
- Vallinotto A., Dodelson S., Zhang P., 2011, *Phys.Rev.D*, 84, 103004
- Wittman D. M., Tyson J. A., Kirkman D., Dell’Antonio I., Bernstein G., 2000, *Nature*, 405, 143